Stratospheric Temperature Climate Data Record from Merged SSU and AMSU-A Observations

CHENG-ZHI ZOU

Center for Satellite Applications and Research, NOAA/NESDIS, College Park, Maryland

HAIFENG QIAN

Earth Resource Technology, Inc., Laurel, Maryland

(Manuscript received 12 January 2016, in final form 13 April 2016)

ABSTRACT

Observations from the Stratospheric Sounding Unit (SSU) on board historical NOAA polar-orbiting satellites have played a vital role in investigations of long-term trends and variability in the middle- and upper-stratospheric temperatures during 1979–2006. The successor to SSU is the Advanced Microwave Sounding Unit-A (AMSU-A) starting from 1998 until the present. Unfortunately, the two observations came from different sets of atmospheric layers, and the SSU weighting functions varied with time and location, posing a challenge to merge them with sufficient accuracy for development of an extended SSU climate data record. This study proposes a variational approach for the merging problem, matching in both temperatures and weighting functions. The approach yields zero means with a small standard deviation and a negligible drift over time in the temperature differences between SSU and its extension to AMSU-A. These features made the approach appealing for reliable detection of long-term climate trends. The approach also matches weighting functions with high accuracy for SSU channels 1 and 2 and reasonable accuracy for channel 3. The total decreases in global mean temperatures found from the merged dataset were from 1.8 K in the middle stratosphere to 2.4 K in the upper stratosphere during 1979–2015. These temperature drops were associated with two segments of piecewise linear cooling trends, with those during the first period (1979–97) being much larger than those of the second period (1998–2015). These differences in temperature trends corresponded well to changes of the atmospheric ozone amount from depletion to recovery during the respective time periods, showing the influence of human decisions on climate change.

1. Introduction

Stratospheric temperature is an essential climate variable in the Global Climate Observing System (WMO 2010). Temperature changes in the stratosphere provide clues on the earth's changing climate for both short-term events and long-term trend. Spikes in stratospheric temperatures lasting about two years occur in response to volcanic eruptions (Hansen et al. 1978, 1993, 1996; Pollack et al. 1976). The solar cycle causes decadal variability in the stratospheric temperature time series (Randel et al. 2009), and increasing greenhouse gases and ozone depletion cool the stratosphere (Manabe and Wetherald 1967; Fels et al. 1980; Hansen et al. 1993; McCormack and Hood 1994; WMO 1999; Shine et al. 2003; Gillett et al. 2011). A long-term stratospheric cooling trend is one of the central indicators of human-induced global climate changes (Thompson et al. 2012).

Satelliteborne sensors are the only means available for providing global temperature observations in the stratosphere (Randel et al. 2009; Seidel et al. 2011; Thompson et al. 2012). The longest observations of the stratospheric temperature were from the Microwave Sounding Unit (MSU) and Stratospheric Sounding Unit (SSU) on board the NOAA TIROS-N polar-orbiting satellite series during 1978–2006 (Kidwell 1998). The MSU had a total of four channels with its channel 4 (57.95 GHz) designed to measure temperatures in the lower stratosphere from 10 to 30 km with a weighting function peaking near 17 km. The SSU was a three-channel

Corresponding author address: Dr. Cheng-Zhi Zou, Center for Satellite Applications and Research, NOAA/NESDIS, NOAA Center for Weather and Climate Prediction, 5830 University Research Court, College Park, MD 20740.
E-mail: cheng-zhi.zou@noaa.gov

DOI: 10.1175/JTECH-D-16-0018.1

© 2016 American Meteorological Society

Unauthenticated | Downloaded 04/04/22 02:43 PM UTC

infrared radiometer measuring temperatures from 20 to 55 km in the middle to upper stratosphere, with their weighting functions roughly peaking near 28, 36, and 45 km, respectively. Since 1998 until the present, the Advanced Microwave Sounding Unit-A (AMSU-A) on board the NOAA-K–NOAA-M (KLM) series, NASA *Aqua*, and European MetOp series have replaced MSU and SSU to provide all-weather, excluding precipitation, temperature observations with higher resolutions both vertically and horizontally. AMSU-A has a total of 15 channels with 6 of them dedicated to measuring temperature profiles from the lower to upper stratosphere. Although these instruments were designed primarily for weather observations, due to continuity and global coverage, together they are the basis for an indispensable climate data record (CDR) for monitoring historical temperature changes from the lower to upper stratosphere.

MSU channel 4 and its companion AMSU-A channel 9 were merged by three groups, the University of Alabama at Huntsville (UAH; Christy et al. 2003), Remote Sensing Systems (RSS; Mears and Wentz 2009), and the NOAA/Center for Satellite Applications and Research (STAR; Zou et al. 2006). These datasets have been extensively used for assessment of temperature trends in the lower stratosphere by the climate science community (Fu et al. 2004; Randel et al. 2009; Seidel et al. 2011; Thompson et al. 2012; Santer et al. 2013; Fu et al. 2015; Seidel et al. 2016). The SSU observations have been processed by two groups: the Met Office (Nash and Saunders 2015) and NOAA (Wang et al. 2012; C.-Z. Zou et al. 2014). The climate trends from the earlier versions of the NOAA and Met Office SSU datasets were found very different, and they also differ significantly from simulated trends from the multiple chemistry–climate and ocean–atmospheric coupled climate models (Thompson et al. 2012). In an effort to reconcile these differences, NOAA and the Met Office developed their respective version 2 SSU datasets (C.-Z. Zou et al. 2014; Nash and Saunders 2015). A recent evaluation suggested that the NOAA version 2 SSU data agree very well with climate model simulations from phase 5 of the Coupled Model Intercomparison Project (CMIP5) in global mean time series and trends (McLandress et al. 2015). In addition to the MSU and SSU climate data records, 11 channels of AMSU-A-only atmospheric-layer temperature time series spanning from the lower troposphere to the upper stratosphere and covering the period from 1998 to present were developed by NOAA (Wang and Zou 2014). Seidel et al. (2016) investigated the stratospheric temperature trend and variability from these separate MSU–AMSU-A, SSU, and AMSU-A time series.

It is desirable to merge the SSU and AMSU-A observations for continued monitoring of the temperature changes in the middle and upper stratosphere from 1979 to present and beyond. This is possible with their 7-yr overlaps from late 1998 to early 2006. However, challenges existed in merging the two observations with accuracy high enough for development of a climate-quality temperature data record. First, the two instruments measured radiation from different atmospheric trace gases—the SSU measures radiation emitted by the stratospheric carbon dioxide (CO_2) within the 15-μm band, while the AMSU-A detects energy emitted by the atmospheric molecular oxygen near the 5.5-mm region. Channels from the two instruments had different sets of weighting functions peaking at different layers of the atmosphere. A physically sound merging requires appropriate matching in their weighting functions so that the resulting time series would come from the same layer of the atmosphere. Unfortunately, weighting functions of the multiple AMSU-A channels do not always provide enough coverage to match with the entire layer of the SSU observations, especially for channel 3. In addition, the SSU weighting functions varied with time and location, making it difficult to find exactly matched AMSU-A observations in all conditions. Second, near-perfect matching of temperatures between the two observations is a necessary condition for the merged time series to be able to reliably detect long-term climate trends. However, their temperature matching tends to have multiple solution problems, since different combinations of the AMSU-A channels may yield the same SSU equivalent channels. Constrained temperature matching is required to generate physically sound merging and to remove calibration biases between observations participating in the merging.

This study proposes a novel variational approach to merging SSU and AMSU-A, matching in both temperatures and weighting functions. We will demonstrate that the approach yields high accuracy in terms of matching of these relevant variables, resulting in physically sound merging of time series for long-term climate trend monitoring with high reliability. McLandress et al. (2015) developed an approach for the global mean merging of SSU and AMSU-A using measurements from high-resolution limb sounders as a transfer standard to remove calibration biases. Our approach here complements their study by providing time- and location-dependent merging with varying SSU weighting functions, yielding a global gridded climate data record with intersatellite biases removed at all grid cells. In addition, this study merges SSU and AMSU-A using their own measurements without relying on other

Unauthenticated | Downloaded 04/04/22 02:43 PM UTC

observations, allowing continuity of the climate data record based only on the operational satellites.

Section 2 introduces the datasets used in this study. Section 3 describes the weighting functions of the SSU and AMSU-A instruments and the challenges in merging them. Section 4 describes the variational approach for merging SSU and AMSU-A. Section 5 presents the major trend results of the merged SSU and AMSU-A time series. Section 6 contains a conclusion.

2. Datasets

The SSU and AMSU-A observations had different scanning geometry and came from satellites with different drifting orbits. Homogenization is required to reconcile these differences before the merger. We use homogenized SSU and AMSU-A datasets for their merger. As a result, no effort for homogenization is needed in this study.

a. SSU dataset

The NOAA SSU version 2 dataset (C.-Z. Zou et al. 2014) was developed based on recalibrated SSU radiances, and it implemented key radiance adjustments for consistent observations that included instrument space-view anomalies, cell pressure decrease over time due to instrument gas leaking, diurnal drift caused by satellite orbital drift, human-induced increase of atmospheric carbon dioxide concentration, and instrument viewing-angle differences. These adjustments converted the original SSU observations to those of nadirlike with fixed cell pressure and atmospheric carbon dioxide concentration. Diurnal drift adjustment was based on scaled diurnal anomalies derived from the NASA MERRA reanalysis (Rienecker et al. 2011), which converted the original SSU observations at different local times to those at 1200 LT (C.-Z. Zou et al. 2014). Intersatellite biases were carefully removed during reprocessing. The structural uncertainty of trends in the data was small, being 0.05, 0.06, and 0.08 K decade^{-1} for global means of channels 1, 2, and 3, respectively (C.-Z. Zou et al. 2014; see Fig. 1 for weighting functions of the three channels). This SSU CDR collects monthly global data from 1979 to 2006 with a grid resolution of 2.5° latitude × 2.5° longitude and is available from the NOAA/STAR website (http://www.star.nesdis.noaa.gov/smcd/emb/mscat/).

b. AMSU-A dataset

The AMSU-A CDR is also from NOAA/STAR (Wang and Zou 2014), which was developed based on the intercalibrated AMSU-A level 1c radiances derived from an integrated microwave intercalibration approach (IMICA, formerly known as the simultaneous nadir overpass method; Zou and Wang 2011). The IMICA calibration minimizes level 1c radiance biases from five different error sources found in the prelaunch operational calibration, including constant intersatellite biases, long-term bias drift, sun-heating-induced instrument temperature variability in radiances, scene temperature dependency in biases due to inaccurate calibration nonlinearity, and biases due to channel frequency shift in certain satellite channels. The IMICA calibrated radiances included observations from *NOAA-15*, *NOAA-16*, *NOAA-17*, *NOAA-18*, *MetOp-A*, and NASA *Aqua* for AMSU-A channels 4–14. Most of these satellites had overlaps with SSU during 1998–2006 except for *NOAA-18* and *MetOp-A*. Additional adjustments were applied to the IMICA intercalibrated radiances for the AMSU-A CDR development in Wang and Zou (2014), including removal of biases due to viewing-angle differences, diurnal drifts for the tropospheric channels 4 and 5 over land and the stratospheric channels 13 and 14 globally, instrument temperature effect, and Earth-location-dependent residual biases. Similar to the SSU CDR, diurnal drift adjustments were based on scaled diurnal anomalies derived from the NASA MERRA reanalysis. After these adjustments, AMSU-A observations at different viewing angles and local observation time were converted to those of nadirlike at 1200 LT. Consequently, the AMSU-A and SSU CDRs can be merged without considering instrumental differences in local observation time and viewing angles.

The 11 channels of the NOAA AMSU-A temperature data cover layers from the lower troposphere to the upper stratosphere. These AMSU-A data are monthly means with a grid resolution of 2.5° latitude × 2.5° longitude covering the period from 1998 to the present for most channels. Unfortunately, channel 14, which is a key channel to merge with SSU, started in 2001 due to the failure of this channel on *NOAA-15*. The AMSU-A data are available from the NOAA/STAR website (http://www.star.nesdis.noaa.gov/smcd/emb/mscat/).

3. The SSU and AMSU-A weighting functions

When the surface contribution is negligible, the atmospheric radiative transfer equation for a satelliteborne radiometer such as SSU and the AMSU-A stratospheric channels is written as

$$R_\lambda = \int_{p_s}^{0} B_\lambda[T(p)]\left[\frac{d\tau_\lambda(p)}{d\ln p}\right] d\ln p, \qquad (1)$$

where R_λ represents the spectral specific intensity or radiance intercepted by a satellite sensor for a channel with wavelength or frequency denoted by the subscript λ, p is the atmospheric pressure, $\tau_\lambda(p)$ is the atmospheric

Unauthenticated | Downloaded 04/04/22 02:43 PM UTC

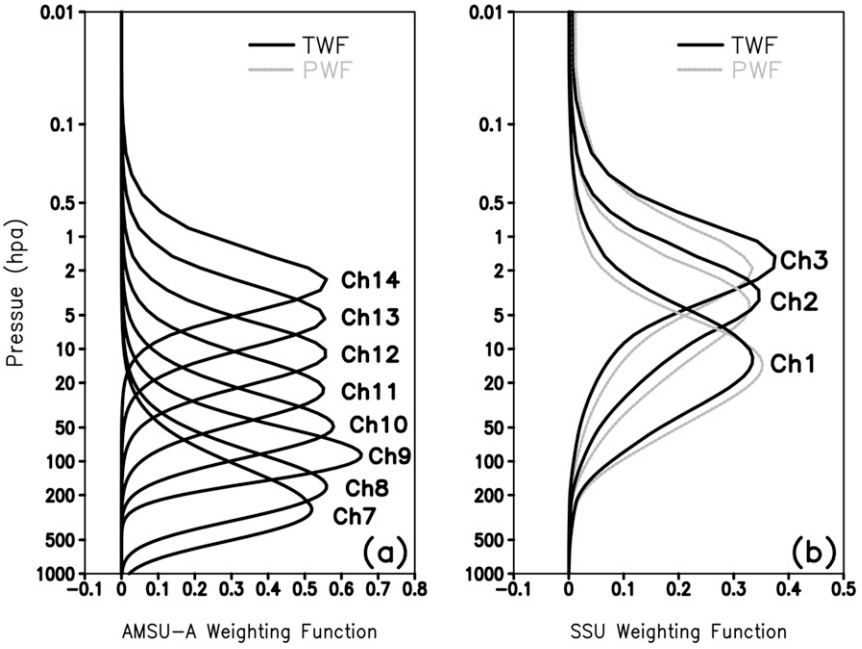

FIG. 1. Planck (gray, PWF) and temperature (black, TWF) weighting functions for (a) AMSU-A and (b) SSU under conditions of the *U.S. Standard Atmosphere, 1976* (COESA 1976). The SSU weighting functions correspond to an atmospheric CO_2 concentration of 330 ppmv and instrument cell pressures of 110, 40, and 15 hPa for channels 1, 2, and 3, respectively. The Planck and temperature weighting functions for AMSU-A are identical.

transmittance, $B_\lambda[T(p)]$ is the Planck function, $T(p)$ is the temperature at the pressure level p, and the subscript s denotes the surface. The vertical derivative of the transmittance, $d\tau_\lambda(p)/d\ln p$, is generally referred to as the Planck weighting function (PWF) for channel λ of the radiometer and its vertical integral from the surface to the top of the atmosphere is equal to one, that is,

$$\int_{p_s}^{0}\left[\frac{d\tau_\lambda(p)}{d\ln p}\right]d\ln p=\tau_\lambda(0)-\tau_\lambda(p_s)=1. \qquad (2)$$

Since the Planck function is a function of wavelength that is different for different instrument channels, its weighting function cannot be directly used for merging observations from different instrumental types. To merge different types of observations, Eq. (1) needs to be transformed to a form with respect to the vertical integral of temperature. For this purpose, with a little manipulation, Eq. (1) is rewritten as

$$\begin{aligned}T_w&=\int_{p_s}^{0}T(p)\left\{\frac{T_b}{R_\lambda}\frac{B_\lambda[T(p)]}{T(p)}\right\}\left[\frac{d\tau_\lambda(p)}{d\ln p}\right]d\ln p\\&=\int_{p_s}^{0}T(p)W_T(p)\,d\ln p,\end{aligned} \qquad (3)$$

where T_b is the brightness temperature, T_w is the weighted mean temperature, and

$$W_T(p)=\frac{T_b}{R_\lambda}\frac{B_\lambda[T(p)]}{T(p)}\frac{d\tau_\lambda(p)}{d\ln p} \qquad (4)$$

is defined as the temperature weighting function (TWF). As seen, $W_T(p)$ is a function of the atmospheric temperatures and of PWF, which is a function of atmospheric trace gases emitting the radiation. Note that both sides of Eq. (1) were multiplied by the same T_b to derive Eqs. (3) and (4). In computing TWFs, T_b on the right-hand side of Eq. (4) is computed by the inverse of the Planck function with observed radiance R_λ. If the temperature profile in the integral of Eq. (3) is the same as those used for computing the TWF in Eq. (4), Eq. (3) would result in a weighted mean temperature exactly the same as the observed T_b. In many applications, however, the temperature profiles in Eq. (3) are from either modeling simulations or retrievals that may be different from those used in calculating the TWFs. This will yield weighted mean temperatures different from the observations. In the merging problem presented in this study, different observations are assumed to be from the same atmosphere—matching errors in temperatures would come from sources other than the temperature profiles. This will be discussed in the next section.

Figure 1 shows the PWF and TWF for AMSU-A channels 7–14 and the three SSU channels under the

Unauthenticated | Downloaded 04/04/22 02:43 PM UTC

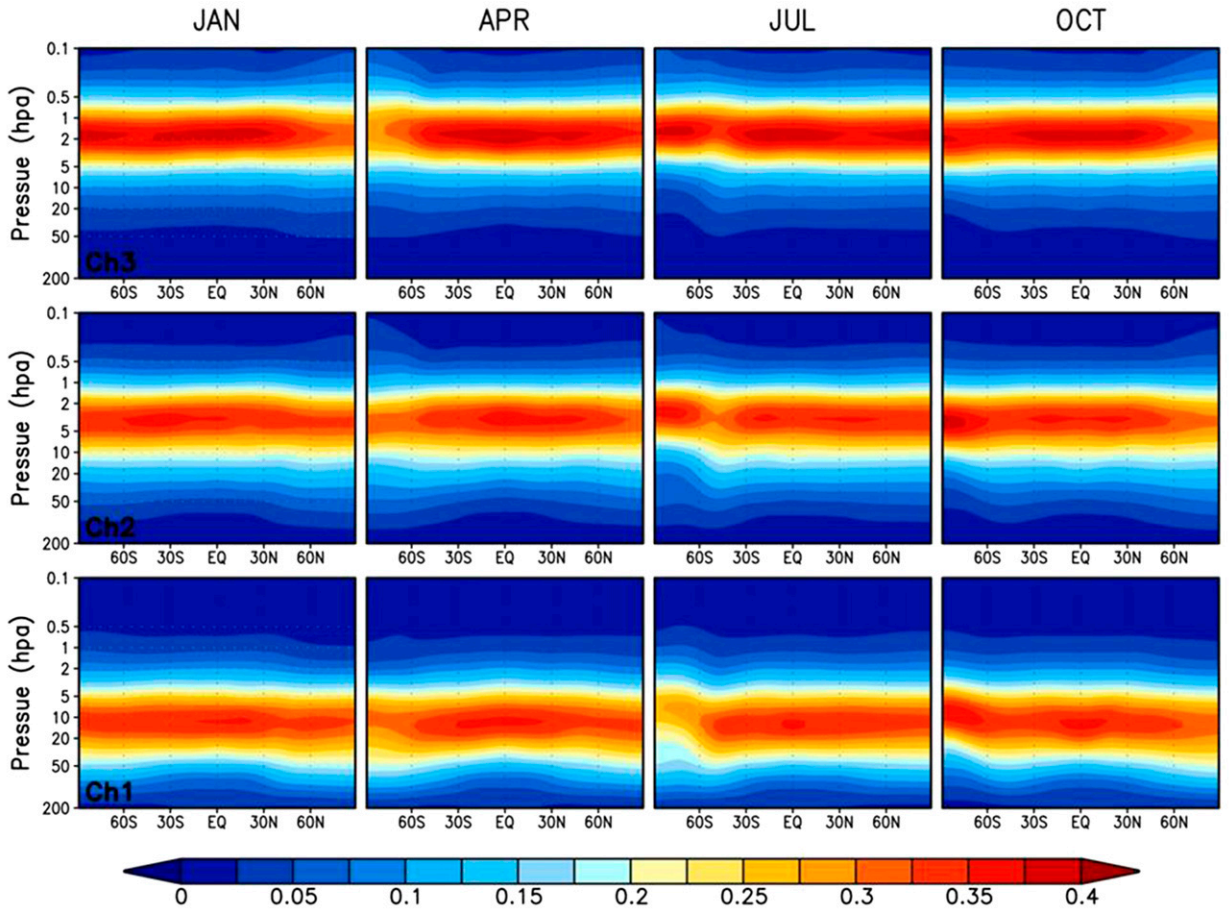

FIG. 2. Monthly mean TWF for the three SSU channels from the MERRA reanalysis as a function of latitude for January, April, July, and October, averaged during 1998–2006.

condition of the *U.S. Standard Atmosphere, 1976* (COESA 1976). In the microwave region, the Planck function is given by the Rayleigh–Jeans approximation, which results in a linear relationship between radiance and brightness temperature. As a result, the AMSU-A PWF and TWF are approximately the same (Fig. 1a). However, because of the nonlinear relationship between temperature and the Planck function in the infrared region, the SSU PWF and TWF are different and they peak at slightly different altitudes (Fig. 1b). For nonstandard atmospheric conditions, their differences can be even larger. Furthermore, unlike the PWF, the vertical integral of the SSU TWF is not necessarily equal to one.

Figure 2 shows changes of the TWF for the three SSU channels with latitude and season calculated using the SSU model within the Community Radiative Transfer Model (CRTM; Chen et al. 2011) with a monthly mean MERRA climatology during 1998–2006, including water vapor, ozone, and temperature profiles, as inputs. Large seasonal changes in the SSU TWF, especially over the polar region, are due to seasonal changes in the atmospheric temperature profiles. In contrast, the SSU PWF (and also the AMSU-A PWF and TWF) remains largely the same with latitude and season (not shown). The insensitivity of PWF to atmospheric conditions is due to the percentage changes with season in the atmospheric trace gases and their transmittance—CO_2 for SSU and O_2 for AMSU-A—are much smaller than those in the temperature. However, since the SSU TWF is to be used to merge with AMSU-A, its larger sensitivity to location and season requires time- and latitude-dependent merging for the best merging result.

4. SSU and AMSU-A merging

a. Merging approach

Merging AMSU-A with SSU requires matching the TWF from the two instruments. Since the TWF of a single SSU channel covers an atmospheric layer much thicker than the TWF of an AMSU-A channel (Fig. 1), several AMSU-A channels are needed to derive an

Unauthenticated | Downloaded 04/04/22 02:43 PM UTC

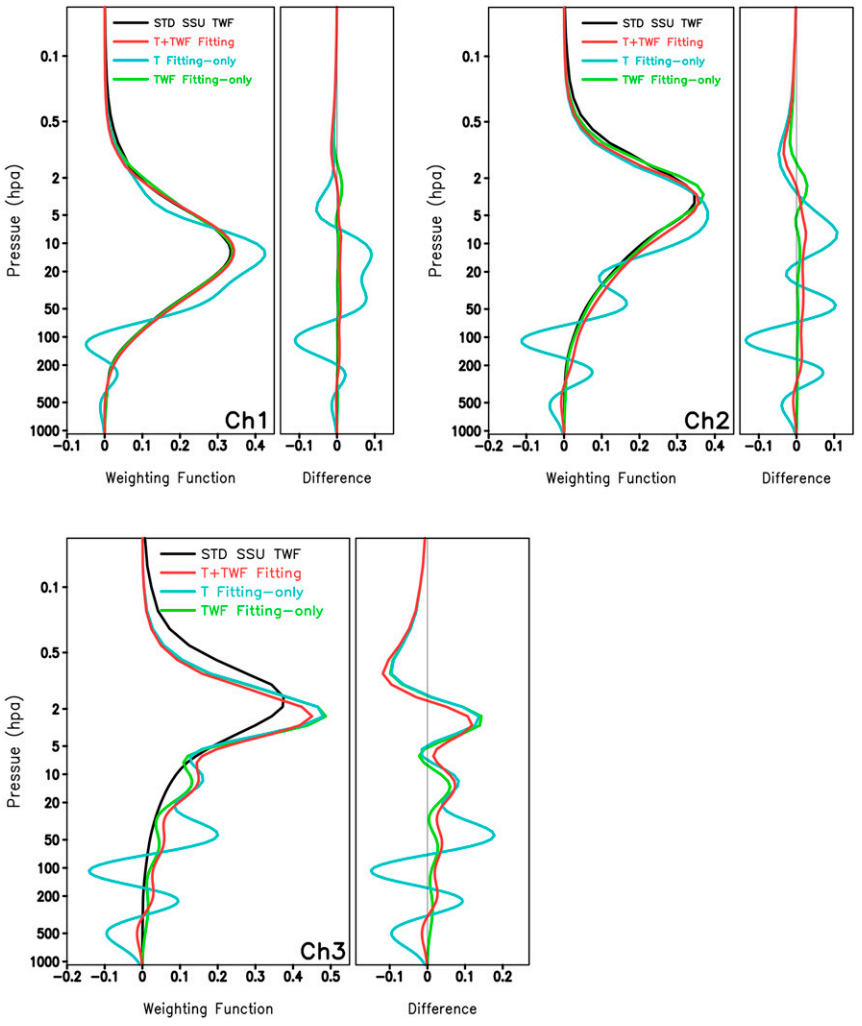

FIG. 3. The standard and fitted TWFs from AMSU-A for the three SSU channels obtained using different fitting approaches in global mean merging. TWF differences between AMSU-A fits and the SSU standard are shown in the right panels.

SSU-equivalent channel. Mathematically, this is to find a $W'_S(p) = \sum_{i=M}^{M+N} a_i W_{Ai}(p)$ to match with the SSU weighting functions in a least squares sense; here $W_{Ai}(p)$ represents the AMSU-A TWFs and $W'_S(p)$ is the derived SSU-equivalent TWF, i is the AMSU-A channel index from channel M through channel $M+N$, and a_i is the matching coefficient for the AMSU-A channel i. The matching is required to satisfy the normalization constraint for the matching coefficients,

$$\overline{W_S} = \sum_{i=M}^{M+N} a_i, \tag{5}$$

where $\overline{W_S}$ is the vertical integral of the SSU TWF and the vertical integral of the AMSU-A TWF is equal to one for the stratospheric channels used in deriving Eq. (5). For simplicity, "SSU extended" or "AMSU-A fit" is used in the following to represent the SSU-equivalent channels derived from the AMSU-A channels. We discuss three merging approaches: "TWF-fitting only" (only TWFs are matched between SSU and AMSU-A without considering temperature matching), "temperature-fitting only" (only temperatures are matched between SSU and AMSU-A without considering TWF matching), and their combined fitting (both TWF and temperatures are matched between the two instruments). The normalization constraint [Eq. (5)] is always satisfied for all these different approaches.

By using as many AMSU-A channels as needed, we were able to derive near-perfect SSU-equivalent TWF, at least for channel 1 (see Table 2; Fig. 3). In theory, when their TWFs are perfectly matched, the SSU and AMSU-A fit should yield identical brightness temperatures under the assumption of no calibration errors. However,

Unauthenticated | Downloaded 04/04/22 02:43 PM UTC

our experiments indicated that the TWF-fitting-only approach resulted in a brightness temperature of AMSU-A fit being different from the original SSU observations around 1–8 K in global means (Table 2), depending on the SSU channels and how many AMSU-A channels were used to derive the AMSU-A fit. There are three possible reasons for this. The first is the calibration errors. The absolute biases of the AMSU-A observations are not exactly known—their accuracy is only known to be around 0.5–1 K, while the SSU observations have a global mean accuracy of about 0.1–0.2 K (C.-Z. Zou et al. 2014). This leads to potential differences of up to 1–1.2 K in global average between SSU and AMSU-A fit even for a perfect matching between their weighting functions. The second reason is TWF error. The TWFs for global mean matching between the SSU and AMSU-A instruments were calculated based on the standard atmosphere. There are no guarantees that TWFs calculated in such a way are an exact representation for global mean temperatures. In addition, the AMSU-A PWF, and thus the TWF, which is identical to PWF, is subject to uncertainty due to the temperature dependency of its absorption coefficients used for the PWF calculation. Consequently, temperature differences between SSU and AMSU-A fit should be expected even for a perfect matching of their TWFs. The third reason is TWF matching error. An imperfect matching of TWF may cause a temperature difference in the fitting. This error is particularly large when AMSU-A channels are insufficient to cover the entire observational layer of an SSU channel, such as channel 3. This error is negligible for SSU channel 1 when the combination of the AMSU-A channels (e.g., 7–14) is good enough to match with its TWF (results are shown in the next subsection).

In addition to the possible errors stated above, the SSU TWFs are also sensitive to seasons and atmospheric conditions (Fig. 2). This makes it impossible for the AMSU-A channels to perfectly match with them in all conditions. Consequently, we seek only for approximate TWF fitting in the sense of minimized differences. On the other hand, an adequate merging must ensure a nearly perfect fit with temperatures. This is a necessary condition if the merged time series is to be used to reliably monitor long-term climate trends. However, temperature fitting alone is not recommended because the solutions are not unique, and, as shown later, it also yields large errors in TWF matching, which cause physically unrealistic merging.

With these considerations, the merging equation for the AMSU-A and SSU observations is designed to minimize the differences of their weighting functions while the statistical errors between their temperature matching are forced to be zero, with a strong constraint of normalization of matching coefficients. This is mathematically expressed as

$$J = (\mathbf{W}_S - \mathbf{W}_\mathbf{A}^\mathrm{T}\mathbf{A})(\mathbf{W}_S - \mathbf{W}_\mathbf{A}^\mathrm{T}\mathbf{A})^\mathrm{T} + \gamma_1(\mathbf{T}_S - \mathbf{T}_\mathbf{A}^\mathrm{T}\mathbf{A})(\mathbf{T}_S - \mathbf{T}_\mathbf{A}^\mathrm{T}\mathbf{A})^\mathrm{T} + 2\gamma_2(\overline{\mathbf{W}_S} - \mathbf{IA}), \quad (6)$$

where J is a cost function that must be minimized for an optimal solution; $\mathbf{A} = (\alpha_M, \alpha_{M+1}, \ldots, \alpha_{M+N})^\mathbf{T}$ denotes the merging coefficients in column vector form for AMSU-A channels from channel M through channel $M+N$ that are used to match a target SSU channel; here the superscript T represents the transformation of a vector or a matrix. The variable $\mathbf{W}_S$ is the SSU TWF of a row vector with respect to height and $\overline{W_S}$ is its vertical integral; $\mathbf{W}_\mathbf{A}$ is a two-dimensional matrix of the AMSU-A TWFs with respect to height (row) and channels M through $M+N$ (column); $\mathbf{T}_S$ is a row vector of the SSU brightness temperatures with respect to the number of data points used as input, and $\mathbf{T}_\mathbf{A}$ is the AMSU-A brightness temperature matrix composed of the number of data points (row) and channels M through $M+N$ (column); $\mathbf{I}$ is a row vector of one; and γ_1 and γ_2 are Lagrangian multipliers.

The above-mentioned construction of the cost function is similar to those described in Goldberg and Fleming (1995) for matching weighting functions from different microwave sounders. In their study, however, the temperature fitting term was expressed as a prescribed noise. By explicitly including the temperature fitting in this study, Eq. (6) allows us to examine the matching of weighting functions and temperatures simultaneously to derive an optimal temperature CDR suitable for climate change detection.

In Eq. (6), $\mathbf{W}_S$, $\mathbf{T}_S$, $\mathbf{W}_\mathbf{A}$, and $\mathbf{T}_\mathbf{A}$ are input variables. Throughout this study, the global gridded monthly SSU and AMSU-A mean layer temperatures ($\mathbf{T}_S$ and $\mathbf{T}_\mathbf{A}$) with a grid resolution of 2.5° latitude × 2.5° longitude during their overlapping period from 2001 to 2006 are used as input. To minimize TWF matching errors, AMSU-A channels 7–14, which have ignorable surface contributions, were used for all three SSU channels. As mentioned earlier, the AMSU-A weighting functions ($\mathbf{W}_\mathbf{A}$) remain largely the same for different atmospheric conditions, so only the set of AMSU-A TWFs corresponding to the standard atmosphere is used as input to Eq. (6) in all experiments in this study.

The solutions of Eq. (6) become those of the TWF-fitting-only method when $\gamma_1 = 0$ and those of the temperature-fitting-only method when γ_1 approaches infinity. The desired solution is to find a limited but nonzero γ_1 by minimizing J with respect to $\mathbf{A}$ subject to the perfect

Unauthenticated | Downloaded 04/04/22 02:43 PM UTC

TABLE 1. Global mean merging coefficients for AMSU-A channels with the T+TWF-fitting approach.

AMSU-A channels	SSU channel 1	SSU channel 2	SSU channel 3
14	0.03	0.36	0.68
13	0.20	0.32	−0.08
12	0.34	0.12	0.31
11	0.25	0.12	−0.07
10	0.12	0.05	0.21
9	0.03	−0.01	−0.12
8	0.04	0.10	0.33
7	−0.01	−0.07	−0.23
Sum	0.9953	0.9965	1.031

fitting of temperatures $[(\mathbf{T}_S - \mathbf{T}_\mathbf{A}^\mathrm{T}\mathbf{A})(\mathbf{T}_S - \mathbf{T}_\mathbf{A}^\mathrm{T}\mathbf{A})^\mathrm{T} = 0]$ and the normalization constraint of the merging coefficients. Unfortunately, such a solution does not exist. In the appendix, we developed a method capable of finding a solution with an optimized fitting in TWF and a minimized error in the temperature fitting. This is referred to as the T+TWF fitting, and it is described in the following.

b. Global mean merging

We first conducted a global mean merging to understand the accuracy of the T+TWF fitting algorithm. In this experiment, a single SSU TWF corresponding to the standard atmosphere (standard TWF) and global mean SSU and AMSU-A temperatures during their overlaps from 2001 to 2006 were used as inputs. Note that although the AMSU-A observations started from 1998, the channel 14 data started only from 2001. Since channel 14 is a key channel for merging all three SSU channels, overlaps during 2001 and 2006 were used for all AMSU-A channels for deriving their merging coefficients throughout the study. The TWFs and the temperatures of the AMSU-A fit obtained from the T+TWF fitting were then compared to the nonpreferred temperature-fitting-only and TWF-fitting-only methods for understanding the advantage of the T+TWF fitting as a merging algorithm.

Table 1 lists the set of AMSU-A merging coefficients for the three SSU channels obtained from the T+TWF fitting. The sum of these coefficients is not exactly equal to one for an SSU channel. This is because, as mentioned earlier, the vertical integral of the SSU TWF, the normalization constraint for the AMSU-A coefficients, is not equal to one. Figure 3 shows TWFs of the AMSU-A fit obtained from different approaches and their differences from the SSU standard TWFs, and Table 2 gives their statistics. As expected, the TWF-fitting-only method resulted in the best TWF fit between SSU and AMSU-A, with the root-mean-square errors (RMSEs) being as small as 0.002 for SSU channel 1 and 0.006 for channel 2. However, the mean temperature differences between SSU and AMSU-A fit (the latter minus the former) were as large as −1.1 K for channel 1 and −2.7 K for channel 2. As discussed earlier, both calibration errors and TWF errors could be responsible for the temperature fitting errors. For SSU channel 3, the TWF fitting is poor, with a larger shift of peaks and large RMSE, being 0.03, an order of magnitude larger than channel 1. As mentioned earlier, this is mainly due to the lack of AMSU-A channels to match with the broad TWF of SSU channel 3, which went through to the upper-stratospheric and lower-mesospheric layers.

The temperature-fitting-only method resulted in the poorest TWF fit with a wiggling shape and shift of peaks from the standard SSU TWF for all three SSU channels. The RMSEs of the TWF in this case were 0.05, 0.06, and 0.10 for SSU channels 1, 2, and 3, respectively. This is an order of magnitude larger than those from the TWF-fitting-only for channels 1 and 2. Although poor in the TWF fit, the mean temperature differences between SSU and AMSU-A fit was zero and the temperature RMSEs are the smallest, being 0.07, 0.10, and 0.14 K for channels 1, 2, and 3,

TABLE 2. Statistics for differences of the weighting functions and temperatures between SSU and the AMSU-A fit for the three different fitting approaches in global mean merging. Differences in TWF between SSU and the AMSU-A fit are zero in all cases and are thus not shown.

	SSU channel	$\mathrm{RMSE}_{\mathrm{TWF}}$	RMSE_T (K)	Bias_T (K) (AMSU-A fit minus SSU)
(T+TWF) fitting	1	0.007	0.082	−0.004
(T+TWF) fitting	2	0.016	0.135	−0.007
(T+TWF) fitting	3	0.057	0.191	−0.009
TWF fitting only	1	0.002	1.097	−1.094
TWF fitting only	2	0.006	2.728	−2.725
TWF fitting only	3	0.035	7.901	−7.900
T fitting only	1	0.048	0.068	−0.000
T fitting only	2	0.055	0.102	−0.000
T fitting only	3	0.101	0.136	−0.000

Unauthenticated | Downloaded 04/04/22 02:43 PM UTC

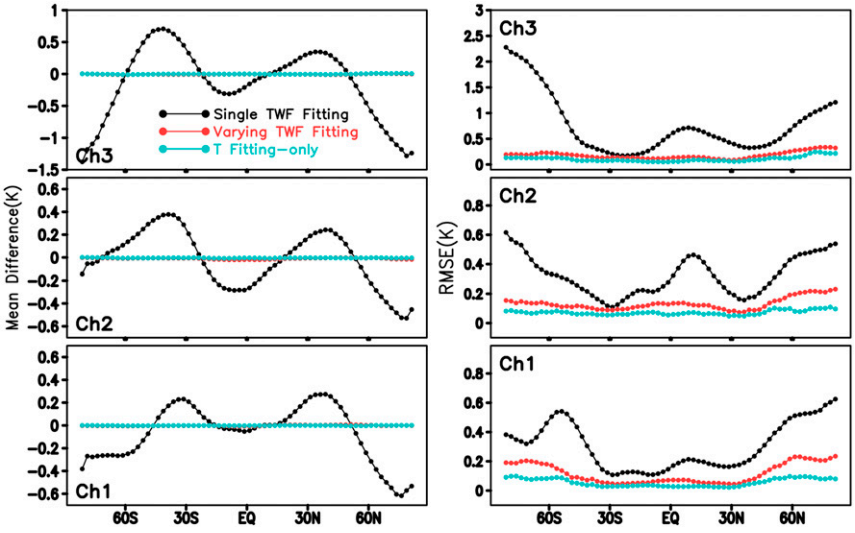

FIG. 4. (left) Zonal mean temperature differences during 2001–06 (AMSU-A fit minus SSU) and (right) their RMSEs for three cases: single TWF fitting (black), varying TWF fitting (red), and temperature fitting only at individual latitudes and months (T fitting only, green). The temperature differences for the varying TWF fitting and T-fitting-only approaches are nearly identical in the left panels.

respectively. This is also expected since, by definition, the temperature-fitting-only approach removes any biases and results in the smallest RMSE between the fitting datasets without considering the TWF fitting. These RMSE values provide a reference for evaluation of the performance of the T+TWF fitting.

The combined T+TWF fitting method gave an intermediate result in terms of RMSE: the RMSE of the TWF is larger than those of the TWF-fitting-only but smaller than those of the temperature-fitting-only method; on the other hand, the RMSE of temperature is significantly smaller than those of the TWF-fitting-only, but it is higher than those of the temperature-fitting-only for approximately 20%, 30%, and 40% for channels 1, 2, and 3, respectively. Notably, the overall shape of the resulting TWF from the T+TWF fitting is very close to the standard SSU TWF, especially for channels 1 and 2 (Fig. 3). This suggested that the standard TWF is very close to the global mean TWF. The other advantage of the T+TWF fitting is that the mean temperature biases between the AMSU-A fit and SSU were zero, as calibration biases between them were absorbed into errors in the TWF fitting. Note that solutions with even smaller RMSE in temperature can be obtained by setting more rigorous criteria for solving the cost function. For instance, one may select a solution with its RMSE of temperature higher than those of the temperature-fitting-only within 10% (see the appendix). However, the trade-off is that the resulting TWF will be closer to those of the temperature-fitting-only, which may not represent the real atmosphere.

Overall, the T+TWF fitting using the selected criteria given in the appendix appeared to result in a satisfactory global mean merging between SSU and AMSU-A in all aspects. In addition, when different SSU TWFs corresponding to the tropical and polar conditions were used as input to the cost function, results similar to those of using the standard SSU TWF inputs were obtained in terms of both the TWF and temperature fitting, suggesting the solution is not so sensitive to the input SSU TWF. This provides good confidence when the approach is used in latitude-dependent merging as shown in the following.

Unfortunately, the single set of merging coefficients obtained in the global mean analysis (Table 1) could not be applied to merging for gridded or zonal mean data. Figure 4 shows the means and RMSE of the zonal mean difference time series between SSU and the AMSU-A fit when the single set of merging coefficients was applied to derive the gridded time series of the AMSU-A fit (referred to as the "single TWF fitting" in the plot and in the following discussion). The figure also shows fitting errors when the temperature-fitting-only approach was used separately for each latitude and month. Similar to global means, the zonal mean temperature-fitting-only resulted in zero differences and the smallest RMSE between SSU and the AMSU fit for all latitudes and months, and thus it provides a reference for understanding the accuracy of the T+TWF fitting. Zonal

Unauthenticated | Downloaded 04/04/22 02:43 PM UTC

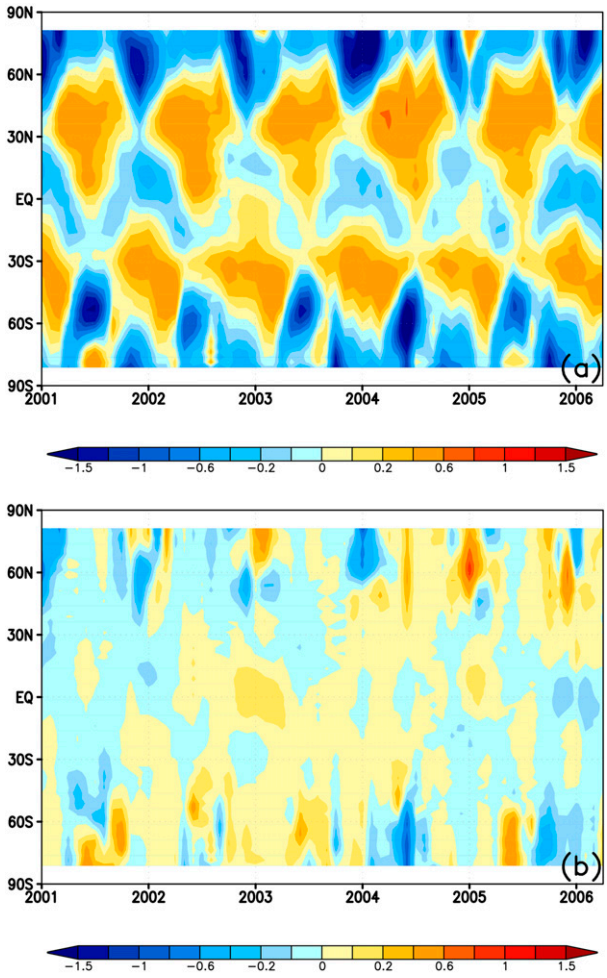

FIG. 5. Latitude–time plots for temperature differences between SSU and AMSU-A fit (the latter minus the former) for channel 1 for the (a) single TWF fitting and (b) varying TWF fitting approaches.

differences for the single TWF fitting are nonzero and they change greatly with latitude with magnitudes up to ±0.2 to ±1 K, depending on channels. In addition, these differences also change with season (Fig. 5a). The RMSE of the single TWF fitting varies with latitude and was on the order of 0.5–2 K over the high latitude for different channels (Fig. 4b). This was nearly an order of magnitude larger than those from the temperature-fitting-only method. These large zonal differences with complex varying features over latitude and time suggested that a single weighting function cannot be used for the global gridded merging between SSU and AMSU-A.

c. *Latitudinal and gridded merging*

To overcome the problem, we conducted month- and latitude-dependent merging, where merging coefficients were allowed to change with month and location in solving the cost function [Eq. (6)], respectively. In this merging, the single standard SSU TWF was still used as a first-guess input for all latitudes and months, but monthly zonal mean SSU and AMSU-A brightness temperatures ($\mathbf{T}_S$ and $\mathbf{T}_A$) for each month and each latitudinal belt were used separately as inputs to the variational Eq. (6) (denoted as ''varying TWF fitting'' in Fig. 4 and the following discussion). As a result, zonal mean merging coefficients varying with latitudes in a 2.5° grid resolution were derived for each month from solving Eq. (6). These coefficients were then applied to derive the AMSU-A fits for the corresponding SSU channels for each latitude and month. Figure 4 shows the mean differences and RMSE of the temperature fitting for the varying TWF fitting in comparison with the single TWF fitting. Contrary to the single TWF fitting, the temperature differences in the varying TWF fitting were zero in all latitudes, the same as those from the temperature-fitting-only approach. The RMSEs of the varying TWF fitting are around 0.1 K in the low latitudes and 0.2 K over the polar region for all three channels. These are higher than those of the temperature-fitting-only for about 30%–100%. In any case, the RMSEs of the varying TWF fitting approach were in a range in which they will not cause large matching errors (defined as the standard deviation divided by the data number in the overlaps) to reduce the merging accuracy and are thus acceptable.

Figure 5b shows the time–latitude plot for differences between the SSU channel 1 and the AMSU-A fit with the varying TWF fitting approach. Channels 2 and 3 were similar in magnitude and pattern and thus are not shown. Differences are around 0.1–0.2 K for most latitudes and months with no seasonal cycles, although they are occasionally larger over the polar region. This is in contrast to those from the single TWF fitting, in which large differences with seasonal cycles occurred (Fig. 5a). These results indicated a satisfactory merging between SSU and AMSU-A for nearly all latitudes and months with the varying TWF fitting.

Figure 6 shows the resulting TWFs of the AMSU-A fits as a function of latitude and month obtained from the varying TWF fitting approach. These TWFs are compared to those calculated from the MERRA reanalysis as shown in Fig. 2. There are many similarities between them. To name a few, the TWF peaks from both plots are approximately the same for channels 1 and 2; both plots show larger TWF values near the South Pole in October for both channels 1 and 2; and both plots show upward shifts of channel 1 peaks in October near the South Pole. These similarities suggested that the

Unauthenticated | Downloaded 04/04/22 02:43 PM UTC

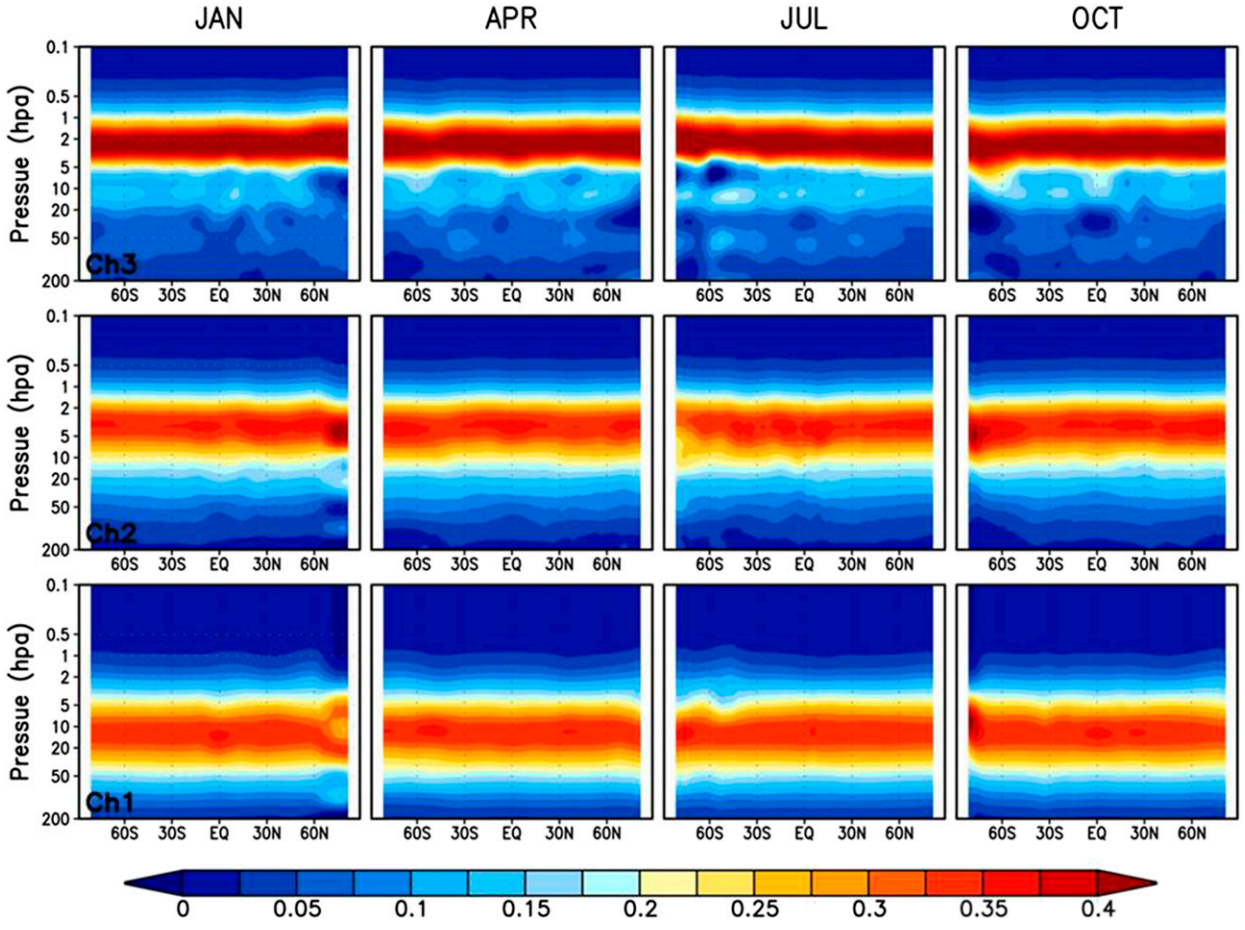

FIG. 6. As in Fig. 2, except that the monthly mean TWF of the AMSU-A fits to the three SSU channels obtained from the varying TWF fitting.

excellent temperature fitting with the varying TWF fitting was based on the TWF fitting with reasonably good accuracies for channels 1 and 2 and thus was physically sound.

For channel 3, the TWF peaks of the AMSU-A fit were slightly lower than those from the MERRA reanalysis. This is similar to the global mean fitting shown in Fig. 3, which occurred due to the lack of AMSU-A channels in the upper stratosphere and lower mesosphere. Despite larger errors in the TWF fitting, the temperature fitting for channel 3 is as good as those for channels 1 and 2. Consequently, trend results from the extended SSU channel 3 are reported similarly to channels 1 and 2 throughout this study. However, cautious views on the representation of the atmospheric layers from channel 3 are recommended, since its TWF fitting error is typically an order of magnitude larger than those of channels 1 and 2.

To avoid noise, no attempt was made to derive weighting functions for the AMSU-A fit at each grid cell. Instead, the monthly zonal mean merging coefficients obtained from the varying TWF fitting were applied to all the grid cells in the corresponding latitudinal belt for the SSU and AMSU-A merging at grid cells. Since the zonal mean weighting function does not necessarily remove intersatellite biases for individual grid cells (Fig. 7a) within a latitudinal belt, additional bias corrections were conducted to remove residual biases at grid cells. This was done by first calculating a yearly mean annual cycle climatology for each grid cell using the 5-yr overlaps during 2001–06 between SSU and the AMSU-A fit (Fig. 7b). This annual cycle climatology has a nonzero mean in general that is different at different grid cells. The annual cycle was then subtracted from the time series of the AMSU-A fit to reduce any potentially larger seasonal variations in their differences from SSU (Fig. 7b). The subtraction also removed the constant mean biases in the AMSU-A fit in the corresponding grid cells, allowing the mean differences between the bias-corrected AMSU-A fit and SSU to be zero for all grid cells during their overlapping period (Fig. 7a).

Unauthenticated | Downloaded 04/04/22 02:43 PM UTC

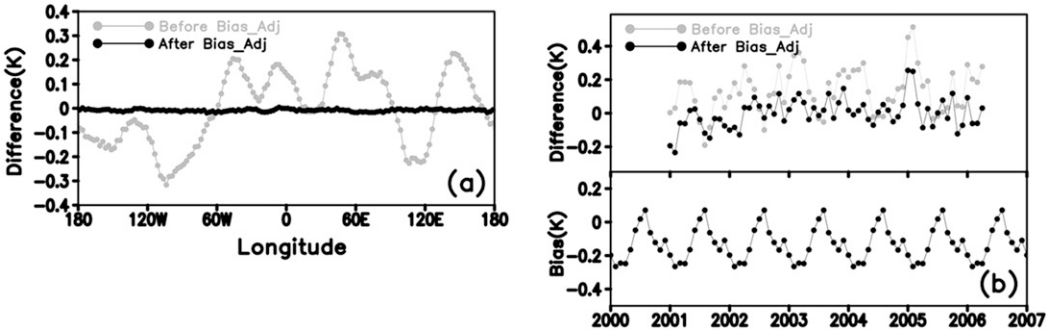

FIG. 7. (a) Mean temperature differences between SSU and AMSU-A fit during 2001–06 for grid cells over the latitudinal belt at the equator (latitude = 0) for before (gray lines) and after (black lines) applying bias corrections at individual grid cells; here the AMSU-A fit was derived using the monthly zonal mean coefficients obtained from the varying TWF fitting approach. (b) An example showing the temperature difference time series between SSU and AMSU-A fit during 2001–06 at the grid cell (lon = 0, lat = 0) (top) before (gray lines) and after (black lines) applying (bottom) an annual cycle climatology with nonzero annual mean.

Finally, the bias-corrected AMSU-A fit was averaged with the SSU to generate a merged CDR at all grid cells.

Figure 8 shows the global mean anomaly time series for the three SSU channels merged with the AMSU-A fits using the varying TWF fitting approach plus bias corrections at individual grid cells, and their difference time series during their overlapping period. For channels 1 and 3, the AMSU-A fit agrees with SSU with zero mean differences, small standard deviation, and negligible drifts over time in their differences. Channel 2 showed a small bias drift over time after 2004, resulting in a slightly larger standard deviation (0.07 K) between SSU and the AMSU-A fit. This drift introduces a 0.1-K error to the channel 2 trend for the entire SSU–AMSU-A observational period, equivalent to a trend

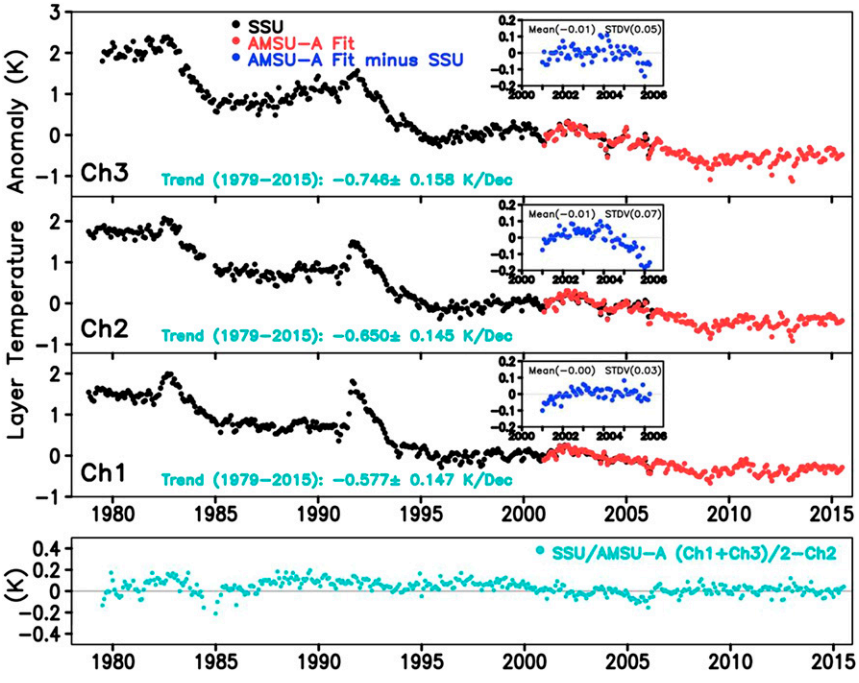

FIG. 8. (top) Global mean temperature anomalies for 1979–2015 for the three SSU channels merged with AMSU-A fits for the varying TWF fitting approach plus gridcell-dependent bias corrections. Their difference time series during their overlapping period are also shown in the corresponding insets. (bottom) Differences between channel 2 anomalies and the average of channel 1 and channel 3 anomalies for the merged data.

Unauthenticated | Downloaded 04/04/22 02:43 PM UTC

TABLE 3. Linear trends (K decade^{-1}) and 2σ uncertainty of the residual time series after the 11-yr solar cycle and aerosol effect were removed from the extended SSU global mean time series.

	1979–2015	1979–97	1998–2015
SSU channel 3	−0.64 (0.06)	−0.93 (0.10)	−0.39 (0.10)
SSU channel 2	−0.55 (0.06)	−0.88 (0.07)	−0.30 (0.10)
SSU channel 1	−0.48 (0.06)	−0.76 (0.07)	−0.25 (0.07)

uncertainty of 0.03 K decade^{-1}. This uncertainty is less than 6% of the charnel trend itself, which is on the order of 0.6–0.8 K decade^{-1}.

5. Major trend results

Figure 8 gives global mean anomaly trends during 1979–2015, that is, −0.58 ± 0.15, −0.65 ± 0.14, and −0.75 ± 0.16 K decade^{-1} for the extended SSU channels 1, 2, and 3, respectively. These trends included the effects from volcano eruptions of the El Chichon in April 1982 and Mt. Pinatubo in June 1991. Trends were slightly smaller when these effects were excluded (Table 3), that is, −0.48 ± 0.06, −0.55 ± 0.06, and −0.64 ± 0.06 K decade^{-1} for channels 1, 2, and 3, respectively. This is equivalent to a total global mean temperature drop from 1.8 K in the middle stratosphere to 2.4 K in the upper stratosphere during the past 37 years. To see the vertical consistency of the three SSU channels, Fig. 8 also shows differences between anomalies of channel 2 and the average of channel 1 and channel 3 in the extended SSU data. It was found that these differences were within 0.2 K for the SSU observations during 1979–2006 (C.-Z. Zou et al. 2014) and within 0.1 K for all the chemistry–climate model simulations during the same period (Seidel et al. 2011). These findings appeared to maintain very well for the merged SSU and AMSU-A observations during 1979–2015. The peak of the SSU channel 3 TWF is slightly higher than those in the AMSU-A fit (Fig. 3). The fact that the trend relationship between the three channels maintained well before and after the merging suggested that this shift in the TWF peaks may not be a big problem for using the extended SSU channel 3 in trend studies.

Figure 9 shows the zonal mean trends during 1979–2015 for the extended SSU channels. Between 40°S and 50°N, the data showed a flat cooling trend for all three SSU channels. The cooling trend decreased toward the South Pole poleward of 40°S; on the other hand, it became larger toward the North Pole poleward of 50°N for all three channels. Figure 10 shows the global spatial trend pattern during the same period of time, which provides insight into the latitudinal structure in trends.

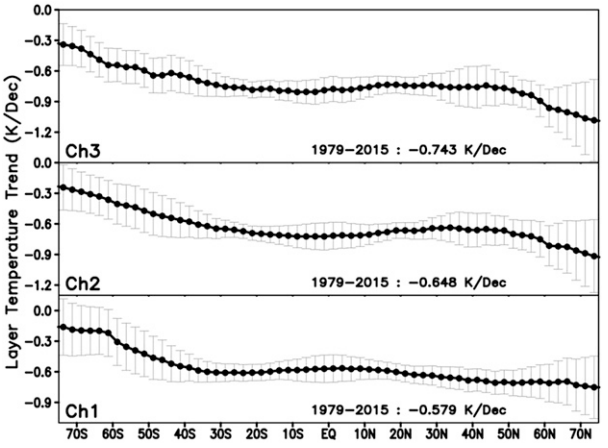

FIG. 9. Zonal mean trends during 1979–2015 for the merged SSU and AMSU-A data. The vertical lines give the uncertainty estimates computed for a 95% confidence interval with autocorrelation adjustment.

Trends are uniform over the tropics and extratropics but have a wave-one pattern for all three channels over the high latitudes in the Northern Hemisphere. The wave-one pattern is characterized by larger cooling over northern Canada/Greenland (50°–150°W) and weaker cooling over Russia/eastern Europe (30°–120°E). This same pattern was also found in the shorter SSU time series during 1979–2006 (C.-Z. Zou et al. 2014). This suggests that the wave-one pattern maybe a persistent feature in the stratospheric temperature trends over the northern polar region, although uncertainty is large due to the larger temperature variability there.

Given that the merged SSU–AMSU-A data span nearly four decades, it is of interest to see how the stratospheric temperature trends respond to an anthropogenic effect, particularly ozone changes from depletion to recovery within the observational period of time (Bourassa et al. 2014). Seidel et al. (2016) investigated trends and variance in the merged MSU–AMSU-A lower-stratospheric temperature time series during 1979–2015 in relation to the solar cycle, El Niño–Southern Oscillation (ENSO), aerosols, and quasi-biennial oscillation (QBO). Randel et al. (2016) analyzed trends and variability during the same period of time for the SSU data merged with the Sounding of the Atmosphere using Broadband Emission Radiometry (SABER) and the *Aura* Microwave Limb Sounder (MLS). Both studies clearly indicated that the observed decadal-scale stratospheric temperature changes during the analyzed period were dominated by the 11-yr solar cycle, the volcanic eruptions of El Chichon and Mt. Pinatubo, and two segments of piecewise linear trends with a separating point around 1997. The piecewise linear

Unauthenticated | Downloaded 04/04/22 02:43 PM UTC

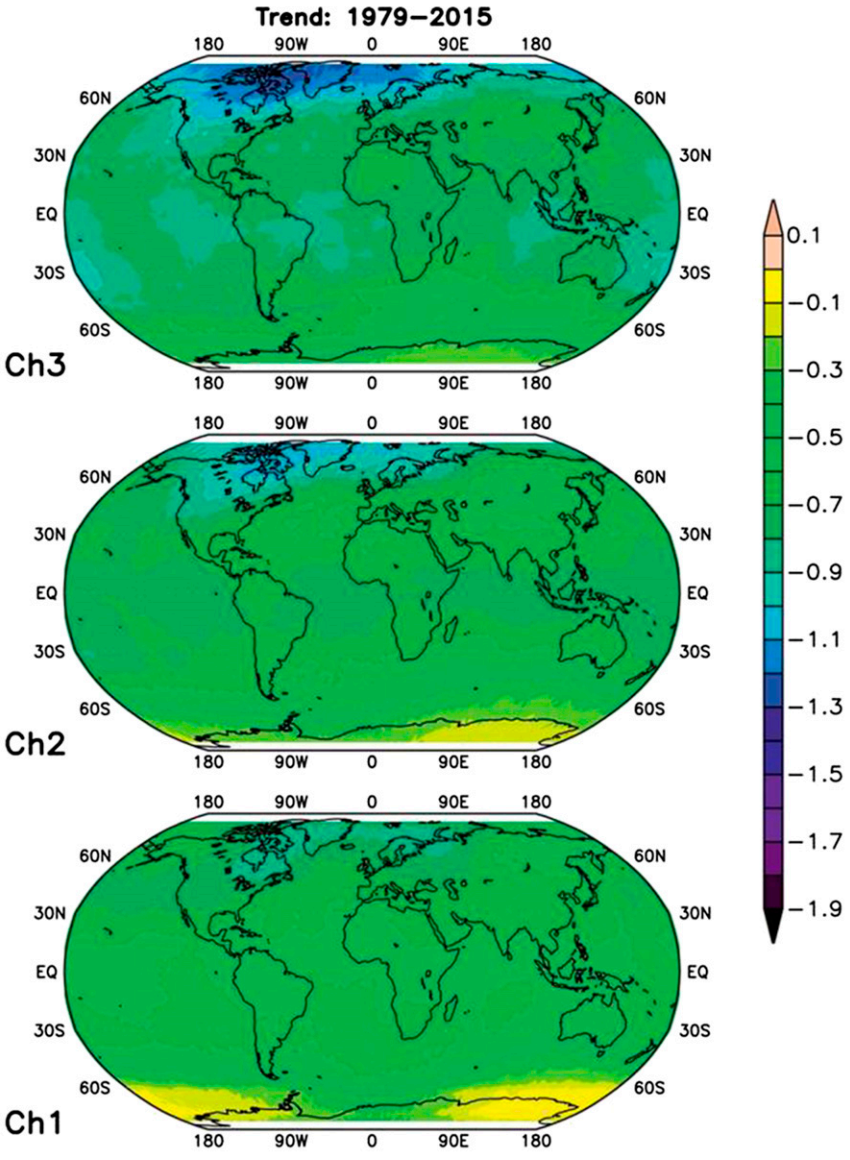

FIG. 10. Spatial trend pattern during 1979–2015 for the SSU–AMSU-A data.

trends were present in both the MSU/AMSU-A lower-stratospheric temperature data and the SSU+MLS extended time series for the middle and upper stratosphere, responding to changes of the atmospheric ozone amount from depletion in the first period (1979–97) to a recovery during the second period (1998–2015; Bourassa et al. 2014). This correspondence between changes in ozone amount and stratospheric temperatures provided strong evidence for influence of human decisions on climate change. Given the significance of its implication, it is important that such a feature be verified by a different observational dataset. Since AMSU-A observations span the same period as that during recovery of the atmospheric ozone, the merging of SSU and AMSU-A provides an ideal dataset for investigating this feature.

To see clearly the piecewise linear trends, we perform a multivariate linear regression analysis for the observational time series to remove decadal-scale variations due to the solar cycle (using the solar F10.7 radio flux as the predictor) and volcano eruptions [using an index of the stratospheric aerosol optical depth from Sato et al. (1993) as the predictor]. The QBO and ENSO are not included in the regression because these interannual variations have a negligible impact on long-term trend calculations. Figure 11 shows the regression results for channel 2. Channels 1 and 3 were similar and

Unauthenticated | Downloaded 04/04/22 02:43 PM UTC

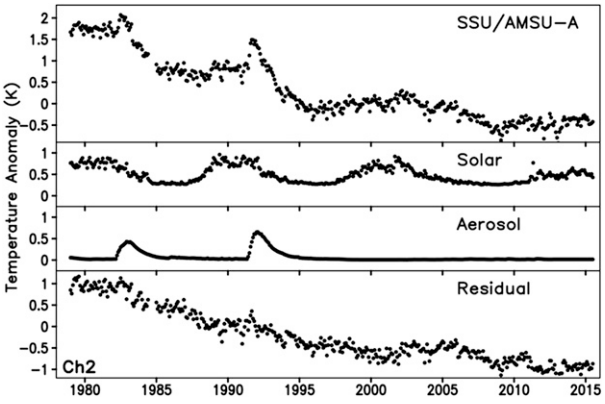

FIG. 11. Time series of temperature anomalies for the extended SSU channel 2, fits to solar cycle and aerosol predictors, and residuals.

thus are not shown. A different aerosol dataset derived by Vernier et al. (2011) with a larger aerosol load post-2000 was also used in the regression to investigate its impact on the residual time series, particularly on the small hump during the 2000–10 period (Fig. 11). However, no major differences were found in the residual time series.

The residual time series in Fig. 11 clearly shows segments of piecewise linear trends with a separating point around 1995–98. Table 3 listed the global mean residual trends during 1979–97 and 1998–2015, and these can be directly compared to results from Randel et al. (2016) using SSU/MLS data. Although trend values are slightly different due to different calculation approaches, the trend differences between the two periods are obvious, providing strong evidence of stratospheric response to human-induced changes of atmospheric trace gases.

6. Conclusions

A variational approach was developed to merge the SSU and AMSU-A observations, accounting for matching in both their temperatures and vertical weighting functions. The approach solves for time- and latitude-dependent merging coefficients from a variational equation specifically designed for the problem. The approach yielded zero mean inter-satellite differences with small RMSE and negligible drift over time in the temperature differences between SSU and the AMSU-A fit during their overlapping period. The solution offers the opportunity for reliable detection of long-term climate trends. Meanwhile, their weighting functions were matched with high accuracy for channels 1 and 2, ensuring the merging is physically sound. Matching accuracy for the weighting function of SSU channel 3 was not as high as for the other two channels due to a lack of AMSU-A channels to cover the upper-stratospheric and lower-mesospheric layers sensed by SSU channel 3. Independent examination of the channel relationship between channel 2 and an average of channels 1 and 3 showed consistency in the merged time series similar to the SSU-only time series. This suggested that matching errors in the channel 3 weighting function may not be a big issue for using its extended time series for climate change studies.

The linear trends of global mean temperatures during 1979–2015 without the volcano eruption effect were −0.48, −0.55, and −0.64 K decade^{-1} for channels 1, 2, and 3, respectively. These trends were associated with two segments of piecewise linear trends during 1979–97 and 1998–2015. Trends of the first period were much larger than those of the second period, corresponding to changes of the atmospheric ozone amount from depletion to recovery during the respective periods of time. This provided strong evidence of an anthropogenic effect on stratospheric climate changes.

AMSU-A was not the only instrument that could extend the SSU data record. Randel et al. (2016) have merged MLS and SABER with SSU using empirical weighting functions to derive a SSU extended time series from 1979 to the present. The hyperspectral infrared sounder, the Atmospheric Infrared Sounder (AIRS) on NASA's *Aqua* satellite, started from 2002 and thus had overlaps with SSU for a few years. Pan et al. (2015) investigated the AIRS stratospheric temperature channels and suggested that they could be used for trend detection in both the global and regional scales with good accuracy. With the available overlaps, it is possible to merge AIRS with SSU to derive an alternative stratospheric temperature CDR. Such a data record may be further extended to the follow-on operational hyperspectral sounders, such as the Infrared Atmospheric Sounding Interferometer (IASI) on board the European MetOp series and the Cross-Track Infrared Sounder (CrIS) on board the *Suomi National Polar-Orbiting Partnership* (*S-NPP*) and the future NOAA Joint Polar Satellite System (JPSS). Since the hyperspectral sounders from the carbon dioxide 15-μm band contain stratospheric channels peaking closely to SSU, their merging is expected to produce an extended SSU channel 3 better than that from the merged SSU and AMSU-A.

On another note, the AMSU-A instruments on board the NOAA and MetOp satellite series are being replaced by the new-generation microwave sounder, the

Unauthenticated | Downloaded 04/04/22 02:43 PM UTC

Advanced Technology Microwave Sounder (ATMS), on board the current *S-NPP* and the future JPSS platforms. The JPSS program will include four more ATMS sensors beyond *S-NPP*. Each JPSS satellite is designed in stable afternoon orbits (1330 LT) for a life cycle of 7 yr, launched every 5 yr, providing at least 2 yr of overlap with the previous satellite. The series of ATMS sensors and CrIS will continue at least until 2038, eventually providing a record of nearly 60 years with extensions from the SSU–AMSU-A. The temperature record from *S-NPP* and JPSS is expected to be exceptionally stable because of the stable orbits and the more advance design of the sensors. Merging algorithms between AMSU-A and ATMS is being investigated. As a first step, X. Zou et al. (2014) developed an algorithm that could optimally resample the ATMS scans with those from the AMSU-A.

With more stratospheric temperature CDRs developed from different observing systems being potentially available, the reliability of the observed stratospheric temperature trends in corresponding to changes in atmospheric ozone and other trace gases may be further improved through mutual validations.

Acknowledgments. We thank Dian Seidel for her review and comments on the manuscript. We also thank the three anonymous reviewers for their constructive comments. The original SSU-only and AMSU-A-only datasets and the merged SSU/AMSU-A dataset are available from the NOAA/STAR website (http://www.star.nesdis.noaa.gov/smcd/emb/mscat/). The work was supported by the NOAA/STAR CalVal Program through the Satellite Meteorology and Climatology Division. The views, opinions, and findings contained in this report are those of the authors and should not be construed as an official National Oceanic and Atmospheric Administration or U.S. government position, policy, or decision.

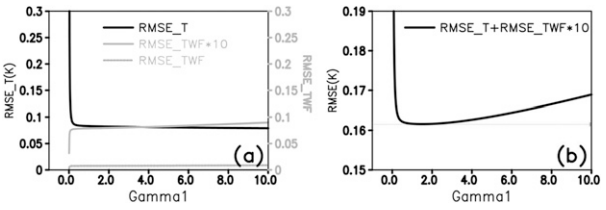

FIG. A1. (a) Change of $RMSE_T$ (K), $RMSE_W$, and a scaled $RMSE_W$ (by 10 times) with γ_1. (b) Change of the combined RMSE ($=RMSE_T + 10 \times RMSE_W$) with γ_1.

APPENDIX

A Method for Finding Optimal Merging Coefficients from the Variational Eq. (6)

Taking derivatives of J in Eq. (6) with respect to $\mathbf{A}$, γ_1, and γ_2 and manipulating the resulting equations, one obtains the following set of coefficients $\mathbf{A}$:

$$\mathbf{A} = (\mathbf{W_A}\mathbf{W_A}^{\mathrm{T}} + \gamma_1\mathbf{T_A}\mathbf{T_A}^{\mathrm{T}})^{-1}(\mathbf{W_A}\mathbf{W_S}^{\mathrm{T}} + \gamma_1\mathbf{T_A}\mathbf{T_S}^{\mathrm{T}} + \gamma_2\mathbf{I}^{\mathrm{T}}) \tag{A1}$$

with constraints

$$(\mathbf{T}_S - \mathbf{T_A}^{\mathrm{T}}\mathbf{A})(\mathbf{T}_S - \mathbf{T_A}^{\mathrm{T}}\mathbf{A})^{\mathrm{T}} = 0 \tag{A2}$$

and

$$\mathbf{IA} = \overline{\mathrm{W}_S}. \tag{A3}$$

Multiplying Eq. (A1) by $\mathbf{I}$ and using the second constraint [Eq. (A3)], one obtains

$$\gamma_2 = [\mathbf{I}(\mathbf{W_A}\mathbf{W_A}^{\mathrm{T}} + \gamma_1\mathbf{T_A}\mathbf{T_A}^{\mathrm{T}})^{-1}\mathbf{I}^{\mathrm{T}}]^{-1}[\overline{\mathrm{W}s} - \mathbf{I}(\mathbf{W_A}\mathbf{W_A}^{\mathrm{T}} + \gamma_1\mathbf{T_A}\mathbf{T_A}^{\mathrm{T}})^{-1}(\mathbf{W_A}\mathbf{W_S}^{\mathrm{T}} + \gamma_1\mathbf{T_A}\mathbf{T_S}^{\mathrm{T}})]. \tag{A4}$$

Note that γ_2 is only a function of γ_1 and the input variables. Substituting Eq. (A4) into Eq. (A1) gives a solution $\mathbf{A}$ that is also a function of γ_1 and the input variables. This solution satisfies the constraint Eq. (A3) for any given γ_1. The solution becomes those of the TWF-fitting-only when $\gamma_1 = 0$ and those of the temperature-fitting-only when γ_1 approaches infinity.

Unfortunately, other analytical solutions that would completely satisfy the temperature constraint [Eq. (A2)] do not exist. To understand this, Figure A1(a) shows a typical behavior of the root-mean-square error between the input temperature ($\mathbf{T}_S$) and its fit ($\mathbf{T_A}^{\mathrm{T}}\mathbf{A}$) [$RMSE_T$, which is the root-mean-square of the constraint term in Eq. (A2)] with changing γ_1. As seen, $RMSE_T$ has its largest value at $\gamma_1 = 0$ and then decreases rapidly with increasing γ_1 to a range that is close to the solution of temperature-fitting-only method. It never equals zero. As a result, one can seek only solutions of $\mathbf{A}$ that approximately satisfy the constraint Eq. (A2).

Figure A1(a) also shows a typical behavior of the root-mean-square error (fitting error) between the input weighting function ($\mathbf{W}_S$) and its fit ($\mathbf{W_A}^{\mathrm{T}}\mathbf{A}$) [$RMSE_W$, which is the root-mean-square of the first term on the right-hand side of Eq. (6)]. Contrary to $RMSE_T$, $RMSE_W$

Unauthenticated | Downloaded 04/04/22 02:43 PM UTC

has its smallest value at $\gamma_1 = 0$, corresponding to the solution of weighting function fitting only, and then it increases rapidly to a range where it changes slowly with increasing γ_1. Although slowly increasing, the $RMSE_W$ may become so large with increasing γ_1 as to cause the weighting function fits physically unreasonable.

A desired solution requires the temperature constraint [Eq. (A2)] to be satisfied as much as possible while the fitting error of the weighting function is as small as possible. Based on this principle, γ_1 should be selected to be large enough so that $RMSE_T$ is close to those from the solution of the temperature-fitting-only, but it shall also be small enough to keep $RMSE_W$ as small as possible. This can be achieved by selecting the smallest γ_1 that allows the $RMSE_T$ to be close to those of the temperature-fitting-only within a prespecified value, say, for example, 30%. This approach worked well for obtaining the desired solutions for global mean merging. For zonal mean merging, however, different threshold values for the $RMSE_T$ are required for different latitudes for the best merging effect. To overcome this difficulty, a more efficient approach was developed to obtain the desired solution. This approach was to search for the minimum of the combined fitting error with changing γ_1, $RMSE = (RMSE_T + \alpha \times RMSE_W)$, where α is an empirical scaling factor. After a few tests, satisfactory results were obtained for all cases investigated in this study, including global mean and zonal mean fittings, when α is selected to be 10 K. This is a value that allows the scaled fitting error of the weighting function, $\alpha \times RMSE_W$, to be comparable to the temperature fitting error [Fig. A1(a)] so that a minimum for the RMSE exists [Fig. A1(b)]. For global mean fitting, the obtained solution using this approach was equivalent to finding the smallest γ_1 that allows the $RMSE_T$ to be close to those of the temperature-fitting-only within 20%, 30%, and 40% for channels 1, 2, and 3, respectively. For zonal mean fitting, the resulting $RMSE_T$ varies from 30% to 100% larger than those of the temperature-fitting-only, depending on channels and latitudes (see the main text).

The sensitivity of the approach to potential calibration errors was investigated by adding random errors in the magnitude of 1 K to channels 7–14 of the input AMSU-A temperatures in the global mean fitting. The resulting merging coefficients for individual AMSU-A channels changed for about 0.01–0.05 from those obtained with the observed AMSU-A temperatures as input (Table 1). However, the combined effect from the merging coefficients—the resulting TWFs and temperatures for the AMSU-A fit—is nearly identical for AMSU-A inputs with and without adding the random errors. This occurred because changes in merging coefficients for individual channels in response to the input random errors tend to cancel out when averaged for deriving the TWF and temperature fits. This suggests robustness of the variational approach in generating consistent merging results.

REFERENCES

Bourassa, A. E., D. A. Degenstein, W. J. Randel, J. M. Zawodny, E. Kyrola, C. A. McLinden, C. E. Sioris, and C. Z. Roth, 2014: Trends in stratospheric ozone derived from merged SAGE II and Odin-OSIRIS satellite observations. *Atmos. Chem. Phys.*, **14**, 6983–6994, doi:10.5194/acp-14-6983-2014.

Chen, Y., Y. Han, Q. Liu, P. V. Delst, and F. Weng, 2011: Community radiative transfer model for Stratospheric Sounding Unit. *J. Atmos. Oceanic Technol.*, **28**, 767–778, doi:10.1175/2010JTECHA1509.1.

Christy, J. R., R. W. Spencer, W. B. Norris, and W. D. Braswell, 2003: Error estimates of version 5.0 of MSU-AMSU bulk atmospheric temperature. *J. Atmos. Oceanic Technol.*, **20**, 613–629, doi:10.1175/1520-0426(2003)20<613:EEOVOM>2.0.CO;2.

COESA, 1976: *U.S. Standard Atmosphere, 1976*. NOAA, 227 pp.

Fels, S. B., J. D. Mahlman, M. D. Schwarzkopf, and R. W. Sinclair, 1980: Stratospheric sensitivity to perturbations in ozone and carbon dioxide: Radiative and dynamical response. *J. Atmos. Sci.*, **37**, 2265–2297, doi:10.1175/1520-0469(1980)037<2265:SSTPIO>2.0.CO;2.

Fu, Q., C. M. Johanson, S. G. Warren, and D. J. Seidel, 2004: Contribution of stratospheric cooling to satellite-inferred tropospheric temperature trends. *Nature*, **429**, 55–58, doi:10.1038/nature02524.

——, P. Lin, S. Solomon, and D. L. Hartmann, 2015: Observational evidence of strengthening of the Brewer-Dobson circulation since 1980. *J. Geophys. Res. Atmos.*, **120**, 10 214–10 228.

Gillett, N. P., and Coauthors, 2011: Attribution of observed changes in stratospheric ozone and temperature. *Atmos. Chem. Phys.*, **11**, 599–609, doi:10.5194/acp-11-599-2011.

Goldberg, M. D., and H. E. Fleming, 1995: An algorithm to generate deep-layer temperatures from microwave satellite observations for the purpose of monitoring climate change. *J. Climate*, **8**, 993–1004, doi:10.1175/1520-0442(1995)008<0993:AATGDL>2.0.CO;2.

Hansen, J. E., W.-C. Wang, and A. A. Lacis, 1978: Mount Agung eruption provides test of a global climatic perturbation. *Science*, **199**, 1065–1068, doi:10.1126/science.199.4333.1065.

——, A. Lacis, R. Ruedy, M. Sato, and H. Wilson, 1993: How sensitive is the world's climate? *Natl. Geogr. Res. Explor.*, **9**, 142–158.

——, and Coauthors, 1996: A Pinatubo climate modeling investigation. *The Mount Pinatubo Eruption: Effects on the Atmosphere and Climate*, G. Fiocco, D. Fuà, and G. Visconti, Eds., NATO ASI Series Vol. 42, Springer-Verlag, 233–272, doi:10.1007/978-3-642-61173-5_20.

Kidwell, K. B., 1998: NOAA polar orbiter data users guide. NOAA. [Available online at http://webapp1.dlib.indiana.edu/virtual_disk_library/index.cgi/4284724/FID2496/podug/index.htm.]

Manabe, S., and R. T. Wetherald, 1967: Thermal equilibrium of the atmosphere with a given distribution of relative humidity. *J. Atmos. Sci.*, **24**, 241–259, doi:10.1175/1520-0469(1967)024<0241:TEOTAW>2.0.CO;2.

McCormack, J. P., and L. L. Hood, 1994: Relationship between ozone and temperature trends in the lower stratosphere:

Unauthenticated | Downloaded 04/04/22 02:43 PM UTC

Latitude and seasonal dependences. *Geophys. Res. Lett.*, **21**, 1615–1618, doi:10.1029/94GL00777.

McLandress, C., T. G. Shepherd, A. I. Jonsson, T. von Clarmann, and B. Funke, 2015: A method for merging nadir-sounding climate records, with an application to the global-mean stratospheric temperature data sets from SSU and AMSU. *Atmos. Chem. Phys.*, **15**, 9271–9284, doi:10.5194/acp-15-9271-2015.

Mears, C. A., and F. J. Wentz, 2009: Construction of the Remote Sensing Systems V3.2 atmospheric temperature records from the MSU and AMSU microwave sounders. *J. Atmos. Oceanic Technol.*, **26**, 1040–1056, doi:10.1175/2008JTECHA1176.1.

Nash, J., and R. Saunders, 2015: A review of Stratospheric Sounding Unit radiance observations for climate trends and reanalyses. *Quart. J. Roy. Meteor. Soc.*, **141**, 2103–2113, doi:10.1002/qj.2505.

Pan, F., X. Huang, L. L. Strow, and H. Guo, 2015: Linear trends and closures of 10-yr observations of AIRS stratospheric channels. *J. Climate*, **28**, 8939–8950, doi:10.1175/JCLI-D-15-0418.1.

Pollack, J. B., O. B. Toon, C. Sagan, A. Summers, B. Baldwin, and W. Van Camp, 1976: Volcanic explosions and climatic change: Theoretical assessment. *J. Geophys. Res.*, **81**, 1071–1083, doi:10.1029/JC081i006p01071.

Randel, W. J., and Coauthors, 2009: An update of observed stratospheric temperature trends. *J. Geophys. Res.*, **114**, D02107, doi:10.1029/2008JD010421.

——, A. K. Smith, F. Wu, C.-Z. Zou, and H. Qian, 2016: Stratospheric temperature trends over 1979–2015 derived from combined SSU, MLS, and SABER satellite observations. *J. Climate*, **29**, 4843–4859, doi:10.1175/JCLI-D-15-0629.1.

Rienecker, M. M., and Coauthors, 2011: MERRA: NASA's Modern-Era Retrospective Analysis for Research and Applications. *J. Climate*, **24**, 3624–3648, doi:10.1175/JCLI-D-11-00015.1.

Santer, B., and Coauthors, 2013: Identifying human influences on atmospheric temperature. *Proc. Natl. Acad. Sci. USA*, **110**, 26–33, doi:10.1073/pnas.1210514109.

Sato, M., J. E. Hansen, M. P. McCormick, and J. B. Pollack, 1993: Stratospheric aerosol optical depth, 1850–1990. *J. Geophys. Res.*, **98**, 22 987–22 994, doi:10.1029/93JD02553.

Seidel, D. J., N. P. Gillett, J. R. Lanzante, K. P. Shine, and P. W. Thorne, 2011: Stratospheric temperature trends: Our evolving understanding. *Wiley Interdiscip. Rev.: Climate Change*, **2**, 592–616, doi:10.1002/wcc.125.

——, and Coauthors, 2016: Stratospheric temperature changes during the satellite era. *J. Geophys. Res. Atmos.*, **121**, 664–681, doi:10.1002/2015JD024039.

Shine, K. P., and Coauthors, 2003: A comparison of model-simulated trends in stratospheric temperatures. *Quart. J. Roy. Meteor. Soc.*, **129**, 1565, doi:10.1256/qj.02.186.

Thompson, D. W. J., and Coauthors, 2012: The mystery of recent stratospheric temperature trends. *Nature*, **491**, 692–697, doi:10.1038/nature11579.

Vernier, J.-P., and Coauthors, 2011: Major influence of tropical volcanic eruptions on the stratospheric aerosol layer during the last decade. *Geophys. Res. Lett.*, **38**, L12807, doi:10.1029/2011GL047563.

Wang, L., C.-Z. Zou, and H. Qian, 2012: Construction of stratospheric temperature data records from Stratospheric Sounding Units. *J. Climate*, **25**, 2931–2946, doi:10.1175/JCLI-D-11-00350.1.

Wang, W., and C.-Z. Zou, 2014: AMSU-A-only atmospheric temperature data records from the lower troposphere to the top of the stratosphere. *J. Atmos. Oceanic Technol.*, **31**, 808–825, doi:10.1175/JTECH-D-13-00134.1.

WMO, 1999: Scientific assessment of ozone depletion: 1998. Global Ozone Research and Monitoring Project Rep. 44, 558 pp.

——, 2010: Implementation plan for the global observing system for climate in support of the UNFCCC (2010 update). GCOS-138, GOOS-184, GTOS-76, WMO/TD-1523, 180 pp. [Available online at http://www.wmo.int/pages/prog/gcos/Publications/gcos-138.pdf.]

Zou, C.-Z., and W. Wang, 2011: Intersatellite calibration of AMSU-A observations for weather and climate applications. *J. Geophys. Res.*, **116**, D23113, doi:10.1029/2011JD016205.

——, M. Goldberg, Z. Cheng, N. Grody, J. Sullivan, C. Cao, and D. Tarpley, 2006: Recalibration of microwave sounding unit for climate studies using simultaneous nadir overpasses. *J. Geophys. Res.*, **111**, D19114, doi:10.1029/2005JD006798.

——, H. Qian, W. Wang, L. Wang, and C. Long, 2014: Recalibration and merging of SSU observations for stratospheric temperature trend studies. *J. Geophys. Res. Atmos.*, **119**, 13 180–13 205, doi:10.1002/2014JD021603.

Zou, X., F. Weng, and H. Yang, 2014: Connecting the time series of microwave sounding observations from AMSU to ATMS for long-term monitoring of climate. *J. Atmos. Oceanic Technol.*, **31**, 2206–2222, doi:10.1175/JTECH-D-13-00232.1.

Unauthenticated | Downloaded 04/04/22 02:43 PM UTC